Cerâmica. 2024, v.70:eZXBR6170 http://dx.doi.org/10.1590/ZXBR6170
ORIGINAL ARTICLE

Evaluation of mix design parameters based on basic constitutive relationships for 3DCP printing

Leonardo de Souza Dias[1*], Marcos A. S. Anjos[2], Marcella S. Barbosa[1], Ulisses T. Bezerra[2]
[1]Federal University of Paraíba, 58051-900, João Pessoa, PB, Brazil
[2]Federal Institute of Education, Science and Technology of Paraíba. 58015-435, João Pessoa, PB, Brazil.

Abstract

Six printing mixtures with variations in cement:sand ratios (in mass) were analyzed, keeping the water/dry material ratio constant, evaluating their printability, considering visual aspects, pumpability and filament integrity. The mixtures were subjected to mini-slump tests, spread on a consistency table, squeeze-flow, and deformation under load of the printed filaments at printing intervals of 0 min, 15 min and 30 min, and then the proportions of the compatible mixtures were determined. with the print. The properties in the hardened state, resistance to bending and compression, adhesion between layers, specific mass and voids index were determined for specimens extracted from printed parts. It was possible to observe that for the printing system used there is an ideal range for these constitutive relationships, and that the mixtures, even with different viscosities, measured according to the squeeze flow, can be printable, provided they meet the ideal ranges for the determined relationships. Regarding the interface of the printed layers, these are critical points of fragility, due to factors such as the formation of regions with voids and loss of surface moisture, which favors the reduction of the mechanical performance of the parts, with the increase in the deposition time.
Keywords: 3DCP, printability, squeeze-flow testing, hardened state, mix design.

INTRODUCTION

Additive manufacturing (AM), also known as 3D printing, has been gaining space and becoming an intensifying tool in the advances of automation in the construction industry. This technology is based on materials joining to develop a three-dimensional structure from a projected digital model. Especially in civil construction, several advantages favor the application of 3DCP concrete printing such as: the increase in architectural complexity that the system provides, cost reduction, among them those related to the use of formwork and production time; conditions linked to worker safety; as well as sustainability factors such as waste reduction [1, 2]. It is estimated that this technology may reduce 30% to 60% of construction waste, 50% to 80% of labor costs, and 50% to 70% of production time [3, 4].

Although promising, the technology of 3D printing cementitious mixtures for construction still presents many challenges at the technical and processing level [2, 5], as no codes or procedures are yet available to test mixtures and new materials or to analyze the structural properties of the cementitious material used for 3D printing [5, 6]. Some works analyzed the properties in the fresh state of the material for 3DCP printing through slump, mini-slump, spread on the consistency table, and squeeze-flow tests [7, 8], while others associated the yield stress, viscosity and thixotropy measurements [9]. In the hardened state, 3DCP specimens are evaluated in cylinders or prisms with dimensions commonly used for cast mortar or concrete, however, there is no standardization in specimen sizes, as can be seen when comparing the specimens employed in the works of Ye et al. [10], Zareiyan and Khoshnevis [11], Zhang et al. [9] and Moelich et al. [12]. However, the application of testing parameters to printed concrete structures from additive manufacturing has not yet been validated [5]. Therefore, this lack of consensus on how to evaluate products and processes for 3DCP printing may create insecurity in investors and end consumers and delay practical applications, especially in countries where the development of this technology is still in the initial stages.

The composition of the materials used for 3DCP printing requires some adjustments of viscosity and yield stress of the cementitious composite to the printing system, so many studies use superplasticizers to reduce the yield stress, facilitating pumping and extrusion. To control viscosity and printing stability, large cement consumption, low water/cement ratios, and high amounts of supplementary cementitious materials (SCM) are used, which causes several works to use aggregate/binder (s/b) ratios between 1.0 and 1.5, and only a few researches use higher ratios, from 1.80 to 2.54. The higher aggregate/binder ratios mentioned above are linked to the greater use of SCM, as can be seen in the literature presented in Table I.

Most works reduced the amount of cement with the inclusion of mineral additions, such as silica fume, fly ash, and blast furnace slag [9, 13, 15, 22, 24], which can

* *leonardo.dias@academico.ufpb.br*
https://orcid.org/0000-0001-6008-3600

Table I: Compilation of compositions from different references.

Reference	Mix cem:sand: w/b	SCM	Other materials	s/b	Cement consumption (kg/m³)
Zhang et al. [9]	1:0.6:0.35	silica fume	-	0.6	≈ 1094
	1:0.8:0.35	silica fume	-	0.8	≈ 1011
	1:1.0:0.35	silica fume	-	1.0	≈ 939
	1:1.2:0.35	silica fume	-	1.2	≈ 877
	1:1.5:0.35	silica fume	-	1.5	≈ 798
Buswell et al. [13]	1:1.47:0.40	fly ash and silica fume	limestone powder	1.47	588
	1:1.47:0.40	fly ash and silica fume	-	1.47	588
	1:1.55:0.28	-	limestone powder	1.55	840
	1:1.55:0.28	-	-	1.55	840
	1:2.45:0.40	fly ash and silica fume	limestone powder	2.45	448
	1:2.54:0.28	-	limestone powder	2.54	640
Ding et al. [14]	1:1:0.305	-	-	1.00	≈ 980
	1:1:0.305	-	recycled sand	1.00	≈ 967
Hasse, et al. [15]	1:1.67:0.41	silica fume	-	1,67	706
Xiao et al. [16]	1:1:0.35	-	-	1.00	≈ 939
	1:1:0.35	-	recycled sand	1.00	≈ 933
Ding et al. [17]	1:1:0.35	-	-	1.00	≈ 947
Ma et al. [18]	1:1.20:0.38	fly ash and silica fume	-	1.20	≈ 726
Marchment and Sanjayan [19]	1:1.5:0.3	fly ash and silica fume	-	1.5	≈ 652
Pham et al. [20]	1:1:0.37	silica fume and blast furnace slag	-	1.0	483*
Rahul and Santhanam [21]	1:1.5:0.40	fly ash	-	1.5	660
Nerella et al. [22]	1:2.2:0.42	-	-	2.2	627
	1:1.8:0.42	fly ash and silica fume	-	1.8	391*
Xiao et al. [23]	1:1:0.35		nano-clay	1.00	320**
Ye et al. [24]	1:0.30:0.55	fly ash and silica fume	-	0.30	655

*≈ approximate value calculated based on the compositions presented by the author; * cement consumption achieved using high levels of SCM; ** cement consumption achieved through the use of high nano-clay content.*

influence the cost of mixtures, in addition to hindering the dissemination of this technology in developing countries or regions without local production of these types of additions, as in the case of northeastern Brazil. Thus, studies with alternative materials that can develop the 3DCP technology using materials with wide local availability are necessary.

Another factor that may hinder the dissemination of this 3DCP technology is that, for the dosage of 3DCP composites, there is a need to study the rheology of these materials through tests that require specific and non-routine equipment in concrete technology. Some works propose dosage methodologies focused on the fluidity of the cement paste and ideal aggregate content, proposing a printing range related to the slump and spread of the mixture [8], or even through more complex tests based on the rheology of the material, through the determination of its yield stress and plastic viscosity [9].

It is known that for 3D printing on concrete, the main test to be performed is buildability, and this is linked to the optimal composition of the 3DCP mixture compatible with the printing system. Furthermore, it is also known that complex rheology-based testing protocols are difficult to access in day-to-day construction. Therefore, the present work aims to

evaluate which are the constitutive relationships for sizing printable 3DCP compositions, based on paste volume to aggregate volume ratio (Vp/Vag), fines consumption (Cf), paste volume (Vp), water to fines ratio (Va/Vf), total aggregate content to mixture (%S), paste volume (Vp) and aggregate to cementitious material ratio (s/b), proposing a dosage method based on these relationships and the printability, shape maintenance and final finish. Batching procedures based on the ratios of Vp/Vag, fines consumption, water consumption, and dosage flowchart, similar to those proposed in this article, are widely used in self-compacting concretes [25, 26, 27] and provided wide development and use of SCC (additive) self-compacting concrete in civil construction.

MATERIALS AND METHODS

The experimental program sought to evaluate which are the constitutive ratios of the compositions that allow printing for the different mixtures evaluated with the variation of the cement: aggregate ratio. First, a reference mixture with a mass ratio of 1:2 (cement:sand) was evaluated, in which the amount of water and additives was varied for the 3DCP printer conditions. The amount of water, superplasticizer, and viscosity modifier additive (VMA) was varied by trial and error until a printable consistency was obtained. Then, the cement: aggregate ratios were varied, keeping the humidity and additives constant and equal to the reference mixture, and the constitutive ratios of the mix were calculated. Finally, the consistency conditions of the printable and non-printable mixtures were evaluated, in addition to the constructability and mechanical properties of the printable mixtures.

Materials: for the materials used to compose the mixtures, washed river sand was employed as the aggregate, in addition to locally produced and sold cement by the manufacturer Cimento Nacional, along with the additives MasterBuilders SCC160 and MasterMatrix UW410 from MBCC Group. These were processed and characterized regarding the main physical aspects, and the tests presented in Table II were performed for each type of material and the respective standards adopted.

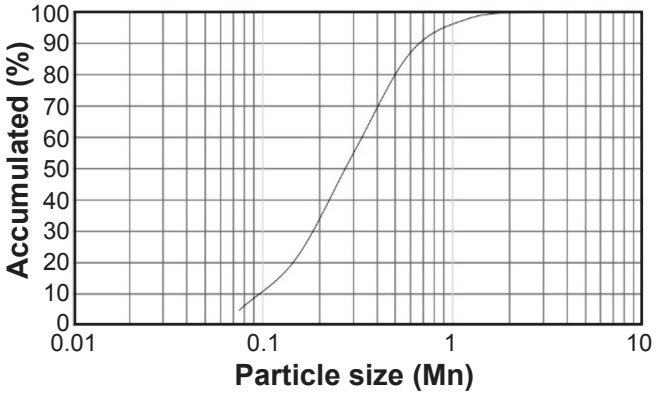

Figure 1: Granulometric characterization of aggregate.

Table II: Parameters of the materials to be studied and their correlated standards.

Materials	Properties	Technical standards
Aggregate	Granulometry	NBR NM 248 [28]/ ASTM D6913[29]
	Specific mass	NBR NM 52 [30]/ ASTM C128[31]
	Unit mass	NBR NM 45 [32]/ ASTM C128[31]
	Percentage of fines	NBR NM 46 [33]/ ASTM C128[31]
Cement and metakaolin	Specific mass	NBR NM 23 [34] /ASTM C188[35] (ABNT, 2000)
	Laser granulometry	-

Table III: Physical properties of aggregate.

Dry specific mass (g/cm³)	Specific mass saturated dry surface (g/cm³)	Specific mass (g/cm³)	Compacted unit mass (g/cm³)	Loose unit mass (g/cm³)	Fineness modulus (%)	Maximum diameter (mm)	Powder content (%)
2.56	2.58	2.61	1.71	1.58	1.42	2.20	4.15

Table III shows the specific mass values found for sand, and the values of the other physical properties found through the tests previously mentioned, unit masses, fineness modulus, maximum diameters of the materials, and powder material content are presented. In addition, the granulometric curve of the material is presented in Figure 1.

Portland cement CP V ARI (equivalent to OPC type III ASTM C 150 and CEM I - EM 197-1) was used, a quick-setting cement without mineral additions, with a specific mass equal to 3.05 g/cm³ and metakaolin, with specific mass equal to 2.49 g/cm³, with average particle diameters of 8.04 µm and 11.69 µm, respectively. Superplasticizer additive (SP) based on polycarboxylates, viscosity modifier additive based on methyl cellulose ether (HPMC), and municipal water were used. The particle size curves of the sand and cement can be seen in Figure 2.

Mix design: the dosage method was based on the determination of the constitutive ratios of the compositions that allowed the impression for the different mixtures evaluated with the variation of the cement:aggregate ratio. To determine the water-to-dry material ratio of the mortar that would allow printing, a first mixture was made with a proportion of 1:2, by mass. The choice of this proportion was based on the values found in the literature, as shown in Table I, in which there is a predominance of 1:1 ratio. Seeking a reduction in cement consumption, it was

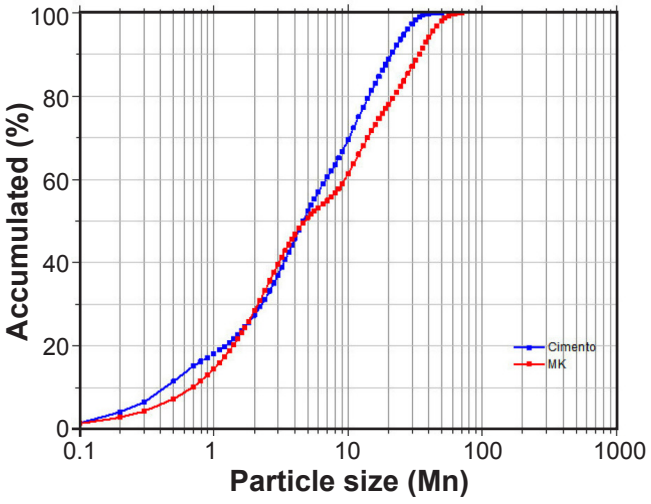

Figure 2: Granulometric characterization of cement and metakaolin.

Figure 3: a) and b) Definition of the optimum water to dry material ratio for the printing conditions, reference mixture (1:2).

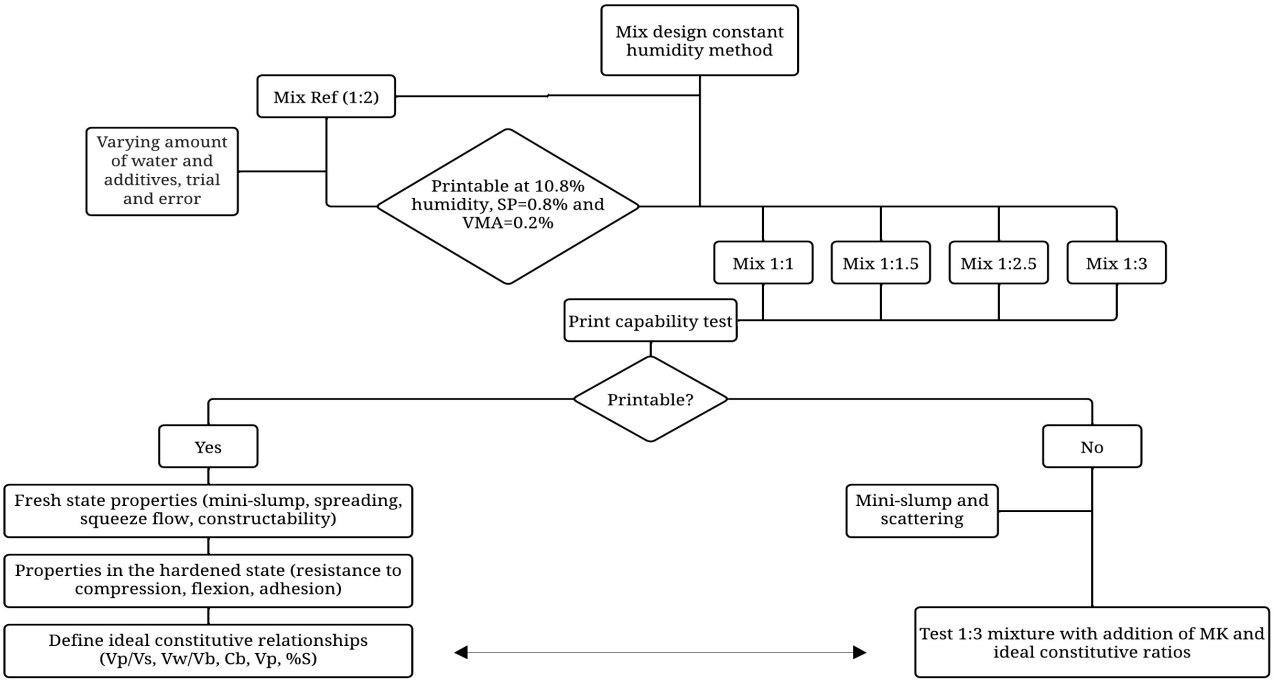

Figure 4: Experimental flowchart.

decided to double the amount of aggregate reaching the selected mix.

Taking into account the printing speed and the extrusion capacity of the 3DCP printer, a variation of water and additives was performed for this composition, by the method of trial and error, until a printable mixture was found, i.e., that allowed the extrusion without clogging the system, that had an entire filament without interruptions along its length and with a limit deformation that allowed the stacking of a new layer, meeting these requirements it was determined the ideal water/dry material ratio (W/Md) and thus be used in other mixtures. This composition with a ratio of 1:2 was printable using a W/Md ratio of 0.108, i.e., 10.8%, 0.89% SP and 0.15% HPMC. A general appearance of the printability of this mixture can be seen in Figure 3, adopted as a reference for the other variations.

Then, these additive ratios and the W/Md ratio were kept constant for the other ratios under analysis in this work, and the cement: aggregate ratios were varied (1:1.0, 1:1.5, 1:2.5 and 1:3.0), keeping the water/dry material ratio and additives constant and equal to the reference mixture, and the constitutive ratios of the mix were calculated, generating the dosage flow presented in Figure 4. Finally, the consistency conditions of the printable and non-printable mixtures were evaluated to recognize their characteristics in their fresh state, as well as the shape retention and mechanical properties of the printable mixtures.

Printing, mixing, and curing system: the printing system designed and built by the authors is a gantry-type printer, presented in Figure 5 with the capacity to print parts with 1.0 m³, which consists of a Cartesian base equipment with mechanized movement in its axes, having an extruder nozzle for deposition of the cementitious material. The printing speed concerning the axes was kept constant at 2500 mm/min and the extrusion rate varied from 25% to 100% of the motor capacity (35 Nm with 82 rpm), being the printing nozzle circular with a diameter of 50 mm, resulting in average thickness and width of the deposited layer of 25 mm and 65 mm, respectively, capable of representing real situations for the dimensions of the filaments, being limited only to the size of the printed structures.

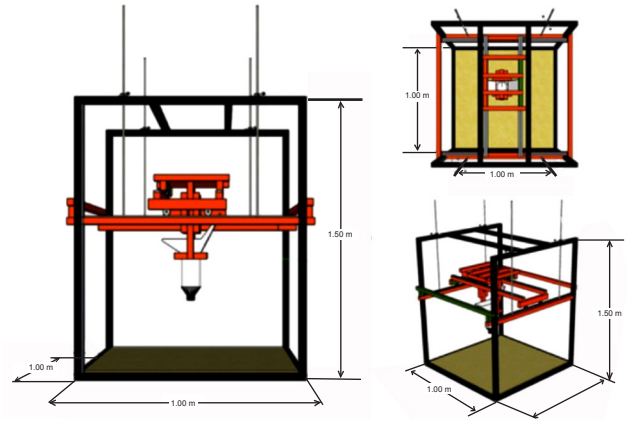

Figure 5: 3DCP printing equipment.

The mixing of the printing materials was performed in an inclined axis mixer (concrete mixer) using the following mixing sequence: in the first moment the homogenization of the dry materials was made by submitting them to about 2 min of rotation; then 70% of the water mass was added keeping the mixture moving for another 2 min; soon after, the superplasticizer was added, continuing the mechanized mixing for 2 min; and then the rest of the water was added, leaving the equipment running until the mortar acquired a homogeneous and slightly fluid aspect; finally, the additive was incorporated into the mixture, being submitted to concreting for another 2 min.

This process was performed in all compositions with ratios and amounts of materials presented in Table IV. A sixth mixture was analyzed to evaluate the validity of the constitutive ratios of the mortars that were considered ideal ranges for the printer's conditions and a given water-to-dry materials ratio of the mixture. This mixture was defined from the addition of 25% of metakaolin in the 1:3.0 mixture and was analyzed only in the fresh state.

Table IV: Compositions adopted.

Mix	Cement (kg/m³)	Sand (kg/m³)	Water (kg/m³)	SP (%)	HPMC (%)	W/Md (%)	A/C (kg/kg)
1:1.0	1085.5	1085.5	234.5	0.89	0.15	10.8	0.22
1:1.5	859.2	1288.8	232.0	0.89	0.15	10.8	0.27
1:2.0	710.4	1420.9	230. 9	0.89	0.15	10.8	0.33
1:2.5	606.3	1515.8	229.2	0.89	0.15	10.8	0.38
1:3.0	528.6	1585.7	228.3	0.89	0.15	10.8	0.43

After mixing, the compositions were printed producing pieces with dimensions of approximately 50 cm in length by 30 cm in height without construction interruption, which were left in two curing conditions for each age analyzed: for the tests of 1 day, the pieces were left exposed to laboratory conditions and for the tests of 28 days, they were left in a laboratory environment for 1 day and 27 days in wet curing by immersion. After these times, specimens were extracted, with dimensions specified in the test standard, for mechanical tests with the aid of a diamond circular saw.

Fluidity and loss of workability: the fluidity test of the mixtures was determined from the mini-cone slump test and the consistency table spread test according to NBR 13276 [36], measured after the mixtures were freshly prepared. The slump test consisted of molding a cone with dimensions of 100 mm at the base and 50 mm at the top, with a height of 150 mm, filled in three layers with compaction of each layer with 15, 10, and 5 blows, successively. Then the cone was removed, and the slump of the mortar was measured. Then, the consistency table was driven with 30 blows in a time of (30 ± 1) s, allowing the mixture to spread freely on the table. After that, the average diameter of the spread mortar was determined in two perpendicular directions measured by a fluidity index, and two repetitions were performed for each test.

To evaluate the loss of workability over time, the slump tests were repeated at intervals of 0 min, 20 min, 10 min, and 5 min, or until the material did not reach slump, which is characterized as the loss of workability, or as many studies present, the open time, which is the instant at which the material does not present extrudability conditions [8-36].

Shape retention: the shape retention was first verified by considering the printing speed of 2500 mm/min (constant), together with the extrusion rate variation (variation for motor rotation capacity) for the different analyzed compositions. In this test, the continuity, deformation, and visual aspect (texture) of a printing layer (Figure 6a) was observed by varying the extrusion rate from 25% to 100% of the motor capacity (35 Nm with 82 rpm) and, with this, it was possible to determine, for each mixture, the ideal printing conditions.

The shape retention condition was the deformation of the layers (Figure 6b), considering a stacking of 5 layers and determining the H_C ratio, according to Equation A. This ratio would be closer to 1, which would imply that there was no deformation of the layers as the print progressed.

$$H_C = \frac{H_R}{H_T} \quad (A)$$

where: H_R= actual height, measured after stacking 5 layers; H_T= theoretical predicted height for the 5 layers, i.e., H_T= 5H; and H is the height of the first layer without top filaments.

Squeeze flow: the squeeze flow test was performed according to the NBR 15839 standard [39], which consists of molding a fresh mortar cylindrical sample with a diameter of 101 mm and height of 10 mm on the clean and dry bottom plate using a plastic ring mold, with subsequent submission of the mixture in the fresh state to a punch conferred by a universal testing machine with a displacement speed of 0.1 mm/s until a maximum displacement of 9 mm or maximum load of 1 kN (whichever is reached first).

Adhesion between the layers as a function of printing time: to investigate the adherence between the layers under the effects of different printing time intervals between the filaments, a 50 cm long piece with two layers was initially printed (Figure 7), where C1 is the first layer that serves as a substrate for C2, the second filament. Samples were extracted from this structure to perform the tests.

Both printed layers of the different specimens were prepared from the same batch of mixture, and these were printed with a deposition delay between C1 and C2 of 0, 15, and 30 min, intervals determined based on the results of the loss of workability test, in which the initial instant of printing and the value in minutes of the maximum and average limit of the mixture that has less open time was adopted. Regarding the dimensions of the tested samples, their length corresponded to 5cm (dimension B of Figure 7), and height and width, sides A and B of Figure 7, respectively, were a function of the natural deformations and spreading of each mixture.

Figure 6: (a) Print speed and print rate determination (b) Printed layers, 1:1.5 mixture

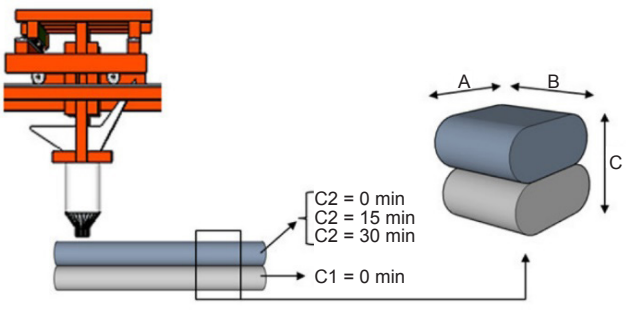

Figure 7: Production and procurement of the samples for the vertical displacement and interlayer adhesion test.

The adherence between the layers was determined based on the tensile strength test by diametrical compression NBR 7222 [40], with the configuration shown in Figure 8, which is commonly adopted in the literature [41-43]. The test was performed on a minimum of three or four samples cut from the initial filament by a diamond disk after seven days of submerged curing. According to Figure 8, two softwood filaments were placed in the interfacial junction region to ensure the correct loading position, which was exerted at a speed of 2.5mm/min.

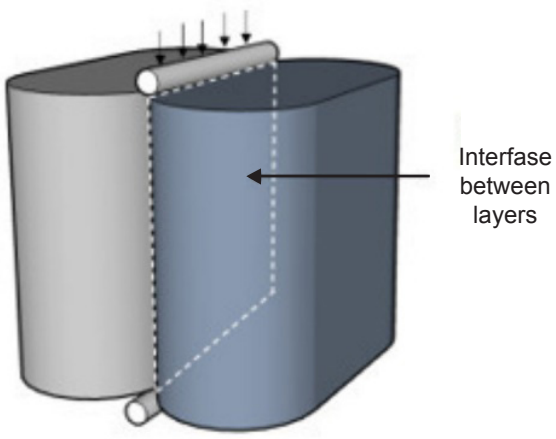

Figure 8: Schematic of the execution of the bond strength test between the layers.

The calculation of the bond strength between the layers as a function of time was performed using Equation B:

$$R_{ad} = \frac{2F}{\pi A} \quad (B)$$

where R_{ad} (MPa) is the bond strength between the layers; F (N) is the ultimate applied load and A (mm²) is the adhered interface area.

Tensile flexural and compressive strength: the mixtures after being printed (in pieces of approximately 50x30 cm) were cut using a diamond cutting disk and water as cutting fluid, after 1 day and 28 days, in dimensions of 40 mm x 40 mm x 160 mm to perform three point bending tests (Figure 9). The cuts of the samples followed two different directions, providing the test in three different test directions, which allowed the evaluation of the anisotropy of the material according to the loading direction concerning the printing direction. For each mixture, 4 specimens were tested with a load speed of 50 N/s according to NBR 13279 [44], being tested in the three directions after 28 days of curing and in the Z axis direction after 1 day of curing. The compressive strength test was performed with the halves resulting from the flexural strength test after rupture, based on NBR 13279 [44], resulting in 8 specimens per mixture. At both ages (1 day and 28 days), these samples were evaluated only in the Fz direction. The test was performed by positioning the support device on the specimen, with dimensions of 40 mm x 40 mm, so that the load was applied in this contact area at a speed of 500 N/s.

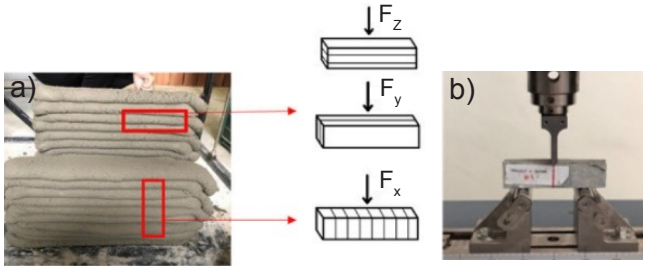

Figure 9: a) direction of extraction and load application; b) example of test setups.

Density and open porosity: the density and porosity of the mixtures printed in the hardened state were evaluated as provided in NBR 9778 [45], following the principle of hydrostatic weighing and comparison of masses in dry and saturated states. For each mixture, prismatic specimens extracted with the aid of a machine with a diamond cutting disk in the dimensions of 40 mm x 40 mm x 160 mm were considered and estimated at 28 days of age.

RESULTS AND DISCUSSION

Fluidity and shape retention: the slump and slump results of the mixtures and the correlation with constitutive parameters such as paste volume (Vp) and water/binder ratio (Va/Vaglo), by volume, of the compositions under analysis can be seen in Figure 10. The spreads and slumps of the analyzed mixtures are different because although the water-to-dry material ratios are equal, the viscosity of the mixture is commanded by the paste volume and

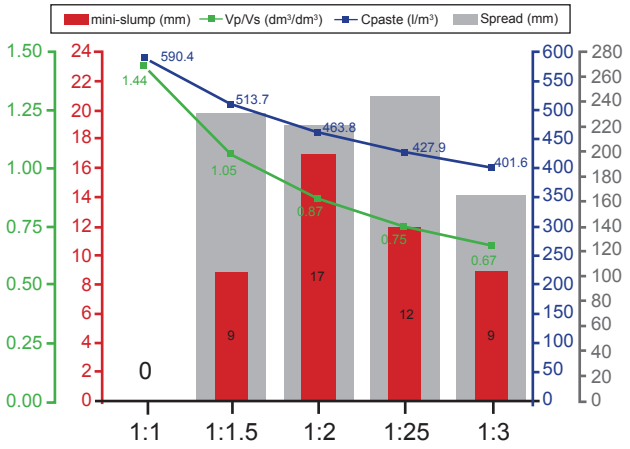

Figure 10: Slump and spreading of the mixture and its Va/Vaglo and Cpaste ratios.

aggregate to binder ratio. Similar tests were conducted by Kaszyńska *et al.* [13], Ma *et al.* [46], Shakor *et al.* [47], and Tay *et al.* [8]. They suggest spreads on the order of 160 mm to 210 mm for printable mixtures, and slump between 4 mm and 8 mm [8]. However, these suggested spreading values cannot be adopted for all printing conditions, as 3DCP printing is conditioned by the printing system (printing speed, extrusion rate, printing nozzle type, and size), mixture viscosity, and aggregate content and particle size.

The 1:1 and 1:3 mixtures were not able to be printed when keeping the water-to-dry material ratios and additive contents constant, even with spreads in the 160 and 210 ranges, because they presented low mobility under the action of external force (extrusion), which reflected in the inability to be built printed parts using the 3DCP printer. There was an insufficient amount of water for particle wetting in the 1:1.0 mixture, due to the high paste content and low water/cement ratio, while the 1:3.0 mixture presented little paste to promote particle mobility by extrusion, considering this specific situation for the printing system used. The mixtures printable in the 3DCP printing system were only the mixtures 1:1.5, 1:2.0, and 1:2.5.

Figures 11 and 12 show the shape retention (Hc) values and appearance for each of the 1:1.5, 1:2.0, and 1:2.5 compositions, respectively. All the printed mixtures show similar Hc and close to 0.9, which may be related to the similar spreads and about 230 ± 15 mm. The 1:1.5 mixture presented a better finish

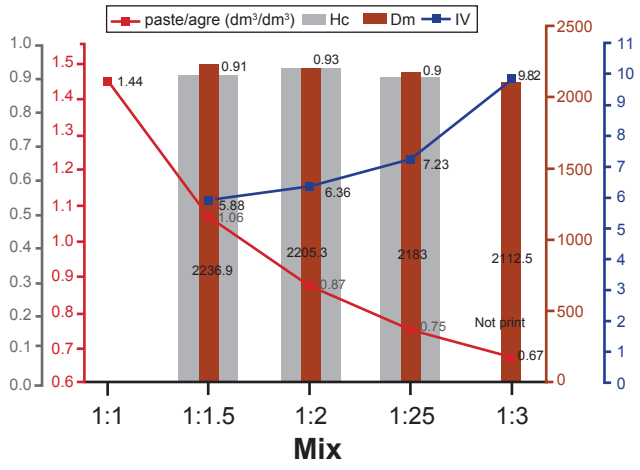

Figure 11: Shape retention and spreading.

Figure 12: Appearance of the printable mixtures: (a) 1:1.5; (b) 1:2.0 and (c) 1:2.5.

without voids and construction cracks, with higher aggregate coverage, due to the higher paste volume to aggregate volume ratio (Vp/Vag), equal to 1.05, while the Vp/Vag values of the 1:2.0 and 1:2.5 mixtures are 0.87 and 0.75, respectively. The 1:2.5 mixture, despite being able to be extruded, was not considered to be of decent quality for printing due to continuity flaws that may be related to its lack of cohesion and workability.

Constitutive relations for mix design: the constitutive ratios of the mixtures presented in Figure 13 show an indication of what the mixtures dosage parameters should be (highlighted region), so that they can be printed under the device printing and extrusion speed conditions, taking into account the constant water/dry material ratio for a reference mixture and the other variations of the aggregate/binder ratios, with the decisions being based on the printable proportions.

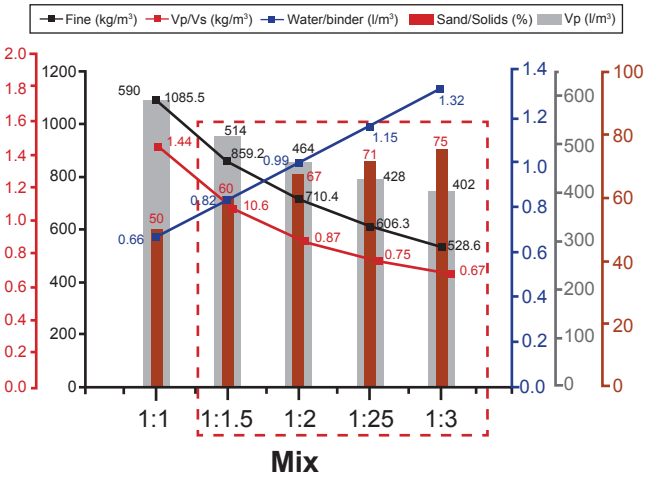

Figure 13: Constitutive parameters of the compositions.

The optimal dosing ranges are presented in Table V, with the most important constitutive ratios for the optimal design for printing, which are related to the paste

Table V: Dosage parameters for printable mixtures.

Paste volume/ aggregate volume (Vp/Vag) (dm³/dm³)	Fines consumption (Cf) (kg/m³)	Water-to-fine ratio (Va/Vf) (l/m³)	Pulp volume (Vp) (l/ m³)	Sand/Solids (%)
0.75 to 1.06	606 to 859	0.82 to 1.15	428 to 514	60 to 71

volume/aggregate volume ratio (Vp/Vag, dm³/dm³), fines consumption (fines, kg/m³), paste volume (Vp, l/m³), water/aggregate volume ratio (Va/Vag, l/m³) and total aggregate/solids ratio of the mixture (sand/solids, %).

However, these values cannot be taken as absolute for diverse types of printers, although they are indicative of a suitable first mix for printing. Therefore, from these constitutive relationships and the dosing flowchart, only minor adjustments would be required to improve print quality by following a dosing flowchart, as shown in Figure 14.

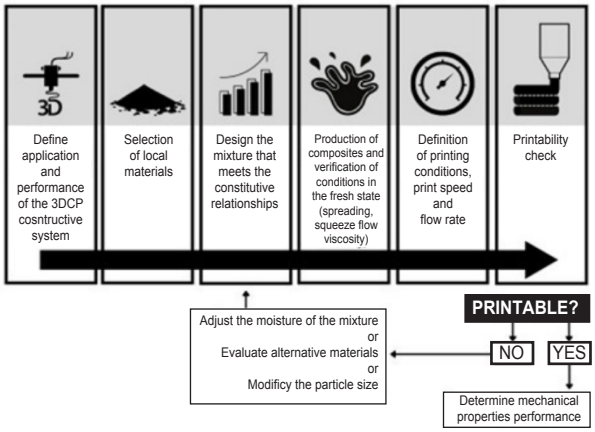

Figure 14: Flowchart for dosing a 3DCP mixture.

To verify the adequacy of the dosage procedure, a 1:0.25:3 composition was evaluated to make the original 1:3.0 mixture, non-printable, fit the dosage parameters of Table III. To do so, metakaolin was added to increase the Vp/Vag ratio, making the constitutive ratios present the following values: Vp/Vag = 0.80, Cf = 615 kg/m³, Va/Vaglo = 0.90, Vp = 443 kg/m³ and sand/total solids = 71%, all within the limits established as fundamental for printing, according to Table V.

Thus, the 1:0.25:3 mixture was printed, with satisfactory printing quality (Figure 15), maintaining the printing conditions, the water-to-dry material ratio

Figure 15: Appearance of the printable 1:0.25:3 mixture.

of the mixture, and additives of the other printable mixtures, which confirms that the printability can be defined by basic constitutive relationships, with great influence of the Vp/Vag ratio, demonstrated that it is possible to increase the amount of aggregates and inert particulates in the mix and thus decrease cement consumption, provided that certain parameters of the composition are met, to promote mobility of the 3DCP composite through an optimized paste content and a granular skeleton to maintain the stability of construction, always correlated with parameters of speed and volume of extrusion.

Squeeze flow: the load-displacement curves obtained after the squeeze flow tests can be seen in Figures 16 and 17. There are two well-defined regions, the first where there is large deformation with a small increase in load (stage II) and the second region where there is small deformation with a large increase in load (stage III), and it is not possible to verify stage I which is related to the elastic-linear behavior [48, 49]. The mixtures with 1:1.5 and 1:2.0 showed long viscous flows with strains of approximately 8.16 mm and 6.05 mm, measured at the transition point from stage II to III, from a tangent straight line drawn superimposed on this viscous phase and measured the transition point. The mixtures 1:2.5 and 1:0.25:3 presented deformations of 4.82 mm and 4.7 mm, which shows lower mobility under load, with the higher sand contents used in these mixtures.

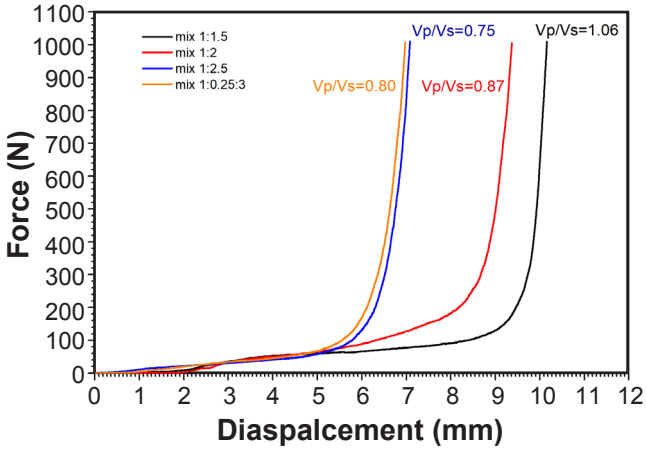

Figure 16: Squeeze flow of the printable samples.

It is possible to observe that the extent of stage II decreases as the proportion of aggregates increases. This behavior of apparent increase in stiffness is related to the emergence of frictional forces due to the geometric restriction of the particles or by the accumulation of solids in the central region between the plates [48]. Furthermore, a transition between stages II and III can be noted with a loading value that decreases with the increment of aggregates, showing once again the influence of the presence of these particles, leading a mixture to have a stiff behavior (1:2.5 and 1:0.25:3), when compared to the other mixtures (1:1.5 and 1:2.0).

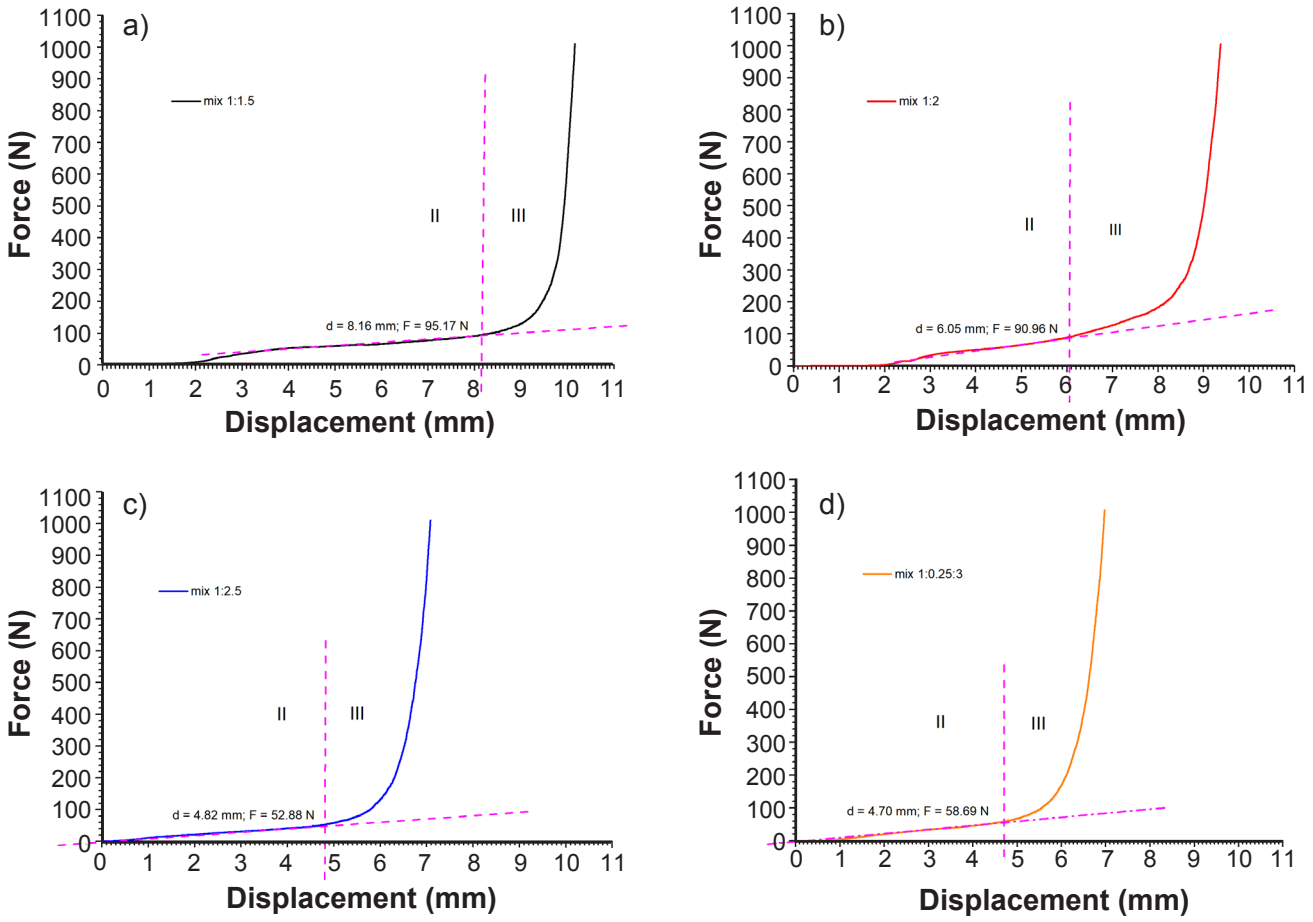

Figure 17: Squeeze flow of the printable samples. a) mix 1:1.5, b) mix 1:2, c) mix 1:2.5, and d) mix 1:0.25:3.

In practical terms, the mixtures that have stages II of greater extension (1:1.5 and 1:2.0) tended to produce filaments with greater deformation and extrusion facilitated by the flow of particles in the system, besides being able to maintain the cohesion of the mixture without segregation of the extrudate, as shown in Figure 12a. As for the mixtures of reduced stage II (1:2.5 and 1:0.25:3), they presented higher stiffness and stability of shape, but, on the other hand, they presented resistance to flow in the extruder tube when compared to the other ratios, and could form filaments with regions of discontinuity, as shown in Figure 12c.

These characteristics can help indications of use according to the properties demanded of the structures, especially about the better finish and pumpability offered by the 1:1.5 and 1:2 mixtures, as in the greater stability provided by the 1:2.5 and 1:0.25:3 mixtures.

The importance of the Vp/Vag ratio for mixture viscosity for 3DCP printing is highlighted since the 1:3.0 composition was not printable due to the low Vp/Vag ratio equal to 0.67. This mixture became printable with the addition of metakaolin (composition 1:0.25:3), which raised the Vp/Vag ratio to 0.8 l/m³ within the range considered ideal for printing for the Vp/Vag parameters between 0.75 and 1.06, keeping the additive contents and W/Md ratio constant.

Figures 16 and 17 demonstrate the influence of the Vp/Vag ratio on the viscous flow behavior, in which it is proven that higher Vp/Vag ratios cause greater deformations due to the lubrication of the aggregate particles causing greater mobility of the mixture, regardless of the Vag/Vaglo ratio. This confirms that the paste is responsible for ensuring cohesion, while keeping the aggregate particles partially separated, lubricating their surface, and reducing frictional forces, which contributes to a relatively easy flow of the system, in contrast to the increase in particle content that provides greater internal friction causing smaller deformations [48, 50]. The mixtures 1:2.5 and 1:0.25:3 showed similar behavior, as they exhibited similar Vp/Vag and Vag/Vaglo ratios, equal to 0.75 and 2.5 and 0.8 and 2.4, respectively. It is worth noting that the rightward deviation of the deformation, verified for the mixture 1:0.25:3, even with the lowest Vp/Vag, may be a result of the nature of the addition, characteristic of its increase in viscosity in cement mixtures.

For the printing system, there is a need for easy flow, which is controlled by the paste. Thus, one can limit the inclusion of larger amounts of sand. Most recent works use binder/sand ratios of 0.8 to 1.5 [9, 14, 16, 17, 24], with the use of high SCM contents. In this work, it was possible to use cement/sand ratios

from 1.0 to 2.5, and a binder/sand ratio equal to 2.4, in the mixture 1:0.25:3, in both cases are higher ratios than the referenced cited and with the use of low contents of regional SCM.

The flowability under load of the 1:0.25:3 mixture was slightly lower than that of the 1:2.5 mixture, but with a better printing quality, keeping the additive contents equal, which may reflect the addition of fines provided by the addition. Thus, the importance of further studies on the quality and printability of mixtures with lower cement consumption is highlighted, as well as the influence of parameters such as roughness, permeable voids, absorption, and specific surface of aggregates and additions, correlating with the levels and types of additives needed for printing.

Tensile flexural and compressive strength: Figure 18 indicates an orthotropic behavior in the mixtures because the flexural strengths in directions Z and Y are equal for the same mixture and different from the strength in direction X, as evidenced by the statistical analysis (Tables VI, VII, and VIII) for all groups with $p < 0.05$, but with the Tukey test showing a non-significant difference between the values in direction Z and Y, as presented in Tables VI, VII, and VIII. It is noted this behavior, because the specimens were extracted adjacent to the direction of impression, having only joints along the impression height, for this reason, the behavior is not anisotropic as verified in other works [9].

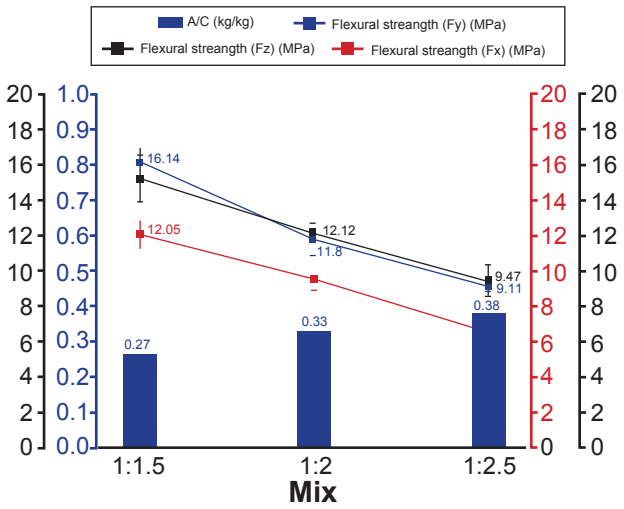

Figure 18: Flexural strength of printed mixtures at 28 days.

There was a reduction in the average flexural strengths in all three directions when comparing the mixtures, this behavior was expected since the increase in aggregate content and amount of water causes a reduction in cement consumption and greater porosity of the mixtures. The levels of resistances are similar

Table VI: Statistical analysis of the mechanical behavior of bending by Anova at Fx Direction and Tukey Test (TT) for each ratio.

Group ratio	Variance	Source of variation	SQ	gl	MQ	F	P-value	F critical	TT 1:1.15	TT 1:2.0	TT 1:2.5
1:1.15	2.23567	Between groups	49.76723	2	24.88361	24.36501	0.001318	5.143253	-	0.06412	0.001077*
1:2.0	0.02963	Within the groups	6.127709	6	1.021285	-	-	-	4.05600	-	0.01536*
1:2.5	0.79854	-	-	-	-	-	-	-	9.82300	5.76700	-

** p-value < 0.05*

Table VII: Statistical analysis of the mechanical behavior of bending by Anova at Fy Direction and Tukey Test (TT) for each ratio.

Group ratio	Variance	Source of variation	SQ	gl	MQ	F	P-value	F critical	TT 1:1.15	TT 1:2.0	TT 1:2.5
1:1.15	0.64566	Between groups	80.42367	2	40.21184	28.47706	0.000866	5.143253	-	0.003809*	0.0008584*
1:2.0	3.53504	Within the groups	8.472469	6	1.412078	-	-	-	7.71400	-	0.25100
1:2.5	0.05551	-	-	-	-	-	-	-	10.24000	2.53100	-

** p-value < 0.05*

Table VIII: Statistical analysis of the mechanical behavior of bending by Anova at Fz Direction and Tukey Test (TT) for each ratio.

Group ratio	Variance	Source of variation	SQ	gl	MQ	F	P-value	F critical	TT 1:1.15	TT 1:2.0	TT 1:2.5
1:1.15	0.61806	Between groups	45.8367	2	22.91835	50.16214	0.00018	5.143253	-	0.009449*	0.0001426*
1:2.0	0.563741	Within the groups	2.741312	6	0.456885	-	-	-	6.40700	-	0.003752*
1:2.5	0.18884	-	-	-	-	-	-	-	14.14000	7.73700	-

** p-value < 0.05*

to those verified by Zang *et al.* [9], who obtained bending stresses on the order of 8.5 MPa to 11.0 MPa, depending on the direction analyzed.

The compressive behavior was determined only in the Z direction, verifying that after 1 day of curing the mixtures 1:2.0 and 1:2.5 have no differences between them, as shown in Figure 19, and the mixture 1:1.5 shows a higher strength than the others, about 17.7% and 21.2%, respectively. The statistical analysis (Tables IX, and X) corroborates this statement, in which all groups have $p < 0.05$, but with the Tukey test showing a non-significant difference between the values of mixtures 1:2.0 and 1:2.5 at both ages. At 28 days the same tendency of the behavior to bending occurs, with increased strength as the cement consumption is increased with lower water/cement ratios, facts proven by higher open porosity of the mixtures with higher water content and lower paste content.

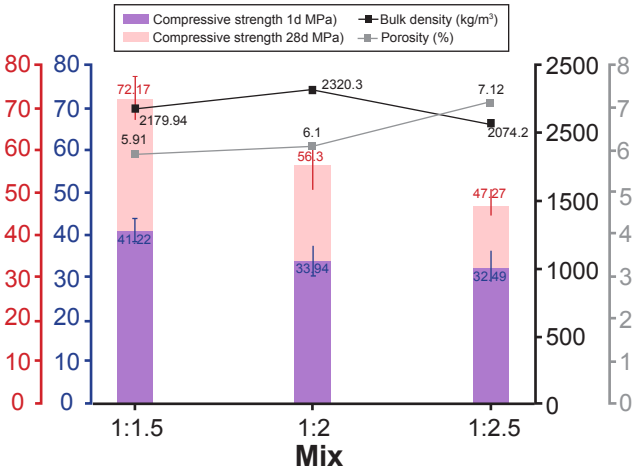

Figure 19: Compressive strength (Fz) of the printable mixtures after 1 and 28 days, and bulk density and porosity at 28 days.

Adhesion between layers as a function of printing time: the results presented in Figure 20 made it possible to define the time intervals to be used to analyze their influence on the bond strength between the layers.

With this result, the intervals between the deposition of the layers were 0 min (T0), corresponding to successive and immediate impressions, 15 min (T15) the intermediate value between the extremes, and 30 min (T30) related to the maximum value reached by the 1:1.5 mixture. This reduced workability value of the 1:1.5 mixture may be a result of the high cement consumption that consequently leads to stiffening with more expressive time when compared to the other proportions.

The influence of mixture compositions and time interval on the bond strength between layers is presented

Table IX: Statistical analysis of the mechanical behavior of bending by Anova at Fx Direction and Tukey Test (TT) for each ratio.

Group ratio	Variance	Source of variation	SQ	gl	MQ	F	P-value	F critical	TT 1:1.15	TT 1:2.0	TT 1:2.5
1:1.15	27.69371	Between groups	1271.7	2	635.85	28.14011	0.000134	4.256495	-	0.009449*	0.0001426*
1:2.0	29.88468	Within the groups	203.3627	9	22.59586	-	-	-	6.693	-	0.003752*
1:2.5	10.20919	-	-	-	-	-	-	-	10.48	3.782	-

** p-value < 0.05*

Table X: Statistical analysis of the mechanical behavior of bending by Anova at Fx Direction and Tukey Test (TT) for each ratio.

Group ratio	Variance	Source of variation	SQ	gl	MQ	F	P-value	F critical	TT 1:1.15	TT 1:2.0	TT 1:2.5
1:1.15	8.23706	Between groups	178.0213	2	89.01063	8.950319	0.009102	4.45897	-	0.03197*	0.01307*
1:2.0	11.33652	Within the groups	79.55974	8	9.944968	-	-	-	4.473	-	0.8436
1:2.5	11.96923	-	-	-	-	-	-	-	5.361	0.7942	-

** p-value < 0.05*

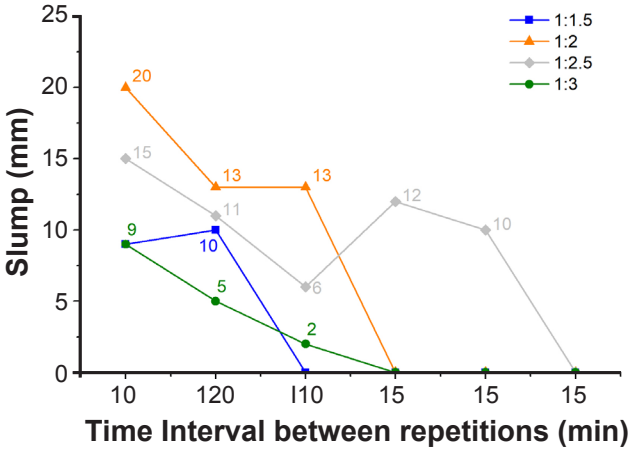

Figure 20: Loss of workability of mixtures (open time).

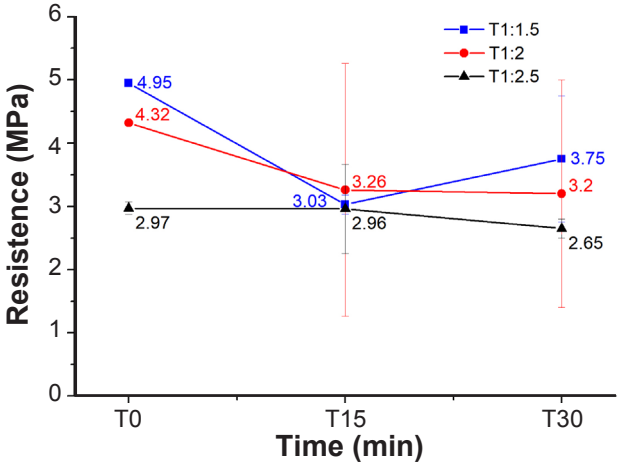

Figure 21 - Bond strength between layers at different intervals.

Table XI: Statistical analysis between mixtures at initial time (T0) by Anova and Tukey Test (TT) for each ratio.

Group ratio	Variance	Source of variation	SQ	gl	MQ	F	P-value	F critical	TT 1:1.15	TT 1:2.0	TT 1:2.5
1:1.15	0.032719	Between groups	15.09998	2	7.549988	55.31025	0.000136	5.143253	-	0.03883	0.000121
1:2.0	0.025696	Within the groups	0.819015	6	0.136503	-	-	-	4.632	-	0.001019
1:2.5	0.351093	-	-	-	-	-	-	-	14.56	9.925	-

in Figure 21, in which a tendency of reduction in adhesion is observed as the paste consumption in the mixture decreases, evidenced mainly at time T0, a phenomenon that was confirmed in the statistical test showing significant difference and p-value < 0.05 (Table XI). For the other instants, there is no significant difference between the results, which presented relatively high errors, which is common to observe in the literature when it comes to this test [51, 52].

Regarding specifically the influence of time on the adhesion between the layers, it was observed a reduction followed by stabilization of the strength with the advancement of time. For all the mixtures, the T0 instant reached the highest stress level, reducing in the other instants (T15 and T30), which statistically have no significant difference between their results (Tables XII, XIII, and XIV), and visually show a relationship of approximate regularity between the times and between the mixtures.

Both behaviors, either between mixtures or with

Table XII: Statistical a nalysis of the mixtures at T0, T15 and T30 by Anova and Tukey Test (TT) for mixture 1:1.5.

Group time	Variance	Source of variation	SQ	gl	MQ	F	P-value	F critical	TT T0	TT T15	TT T30
T0	0.02094	Between groups	13.79339	2	6.896696	6.113745	0.035668	5.143253	-	0.03113	0.1561
T15	0.785404	Within the groups	6.768384	6	1.128064	-	-	-	4.893	-	0.4488
T30	1.359539	-	-	-	-	-	-	-	3.065	1.828	-

Table XIII: Statistical analysis of the mixtures at T0, T15 and T30 by Anova and Tukey Test (TT) for mixture 1:2.0.

Group time	Variance	Source of variation	SQ	gl	MQ	F	P-value	F critical	TT T0	TT T15	TT T30
T0	0.016445	Between groups	5.80339	2	2.901695	1.560021	0.28475	5.143253	-	0.3623	0.3266
T15	2.051158	Within the groups	11.16021	6	1.860035	-	-	-	2.098	-	0.9957
T30	1.503665	-	-	-	-	-	-	-	2.223	0.1249	-

Table XIV: Statistical analysis of the mixtures at T0, T15 and T30 by Anova and Tukey Test (TT) for mixture 1:2.5.

Group time	Variance	Source of variation	SQ	gl	MQ	F	P-value	F critical	TT T0	TT T15	TT T30
T0	0.224699	Between groups	0.437254	2	0.218627	0.926077	0.446157	5.143253	-	0.5486	0.4728
T15	0.1841	Within the groups	1.416471	6	0.236079	-	-	-	1.555	-	0.9885
T30	0.044472	-	-	-	-	-	-	-	1.76	0.205	-

the advancement of time, were expected as presented in the literature [19, 34, 51, 52]. The gain in strength between the ratios can be facilitated by the increase in paste volume that, according to the results of squeeze flow (Figures 16 and 17), enables the printing of parts with lower stiffness and, consequently, a greater area of continuous contact between the layers, expanding the effective bond area, easily visualized in Figure 12. Moreover, there is, allied to this increase in paste volume, the amount of hydration products at the filament interfaces, which tends to be higher, providing a gain in bond strength [19, 53].

This reduction in strength with increasing time intervals between layer deposition becomes an important parameter for analysis, since the interval between the possibility of an adequate layer bond and a gain in strength and stiffness of the filament that avoids large deformations should be recognized. This behavior of decreasing adhesion was also mentioned in the studies of Le *et al.* [34] and Panda *et al.* [51], with instant T0 achieving the highest performance, whereas the stability of the results with longer instants was addressed by Wolfs, Bos, and Salet [52] who performed tests with more advanced intervals (1 h, 4 h, 7 h, and 24 h) and find statistically approximate results.

A possible explanation for this phenomenon is the surface moisture exchange of the filaments, since over time the bottom layer becomes drier tending to absorb more water from the underlying layer and also, some of the air present inside the bottom layer is released

and gets trapped at the interface of the layers which may reduce the effective area of adhesion [51].

CONCLUSIONS

An automated printer in its printing axes was designed and built to provide prints of cementitious mixtures, and to evaluate the constitutive parameters of 3DCP traces with materials commonly used in construction, and thus propose a dosage approach based on the constant dry water/materials ratio of the compositions and variation in the other proportions of the constituent materials, evaluating the properties in the fresh and hardened state most usual for 3D printing in concrete. The following specific conclusions are: i) dosing criteria based on a printable mixture and on varying the composition while maintaining the water to dry material ratio and other constitutive ratios of mixtures based on Vp/Vag and Va/Vaglo seem to be adequate for the dosage of printable mixtures with different strengths and cement consumption; ii) the definition of printing criteria based on slump and spread on a consistency table were not adequate for a dosage definition of the mixtures, being good indicators the squeeze flow and mainly the parameters of the printing system; iii) the developed 3D printer based on extrusion of the printing material meets basic requirements of the 3DCP construction, allowing to evaluate the construction from the deposition of layers continuously; iv) the optimal dosage of 3DCP mixtures seems to be related to the paste volume/aggregate volume ratio (Vp/Vag) between 0.75 and 1.06, fines consumption (kg/m³) between 606 and 859, water to aggregate volume ratio (Va/Vag) between 0.82 and 1.15 l/m³ and total aggregate/solids ratio of the mixture between 60% and 71%; v) Vp/Vag ratios above 0.87, associated with ag/agglomerate ratios lower than 2 provide higher viscous flow of the mixtures in squeeze flow tests. However, mixtures with lower viscous flow thresholds can be printable provided they have adequate Vp/Vag ratios, as achieved in changing the parameters of the 1:3 mixture with the use of metakaolin; vi) the bending behavior and statistical tests confirm the influence of the printing direction on the variability of the measured strength; vii) the adherence between the layers was influenced both by the paste consumption of the mixtures and by the advancement of time between the depositions, being observed low alteration in more advanced intervals, which becomes a positive behavior when turned to practical terms, being able to enable greater freedom in controlling the deposition time between the layers; and viii) the compressive strengths of 3DCP mixtures are relatively high when compared to concretes generally used in construction, and are associated with high cement consumption, but there is no statistical difference between mixtures 1:2.0 and 1:2.5. The present study presents an indication that the constitutive ratios of the mixtures are fundamental to define the compositions, and that the Vp/Vag, Va/Vaglo and sand/total solids ratios command the behavior of the impression. However, further investigations are necessary, especially related to the influence of the type and percentage of SCM, considering the local availability, the granulometry of sand and its replacement by low cost particulate material, as well as the evaluation of the impression in larger sizes. Investigations in this direction are being conducted by the authors, starting with the construction of a printer with higher printing capacity, which will be able to evaluate full-scale prototypes.

ACKNOWLEDGMENTS

The authors thank the support provided by the institutions IFPB and UFPB, as well as UFRN, Coordenação de Aperfeiçoamento de Pessoal de Nível Superior (CAPES), Fundação de Apoio a Pesquisa da Paraíba (FAPESQ), and Conselho Nacional de Desenvolvimento Científico e Tecnológico (CNPQ).

REFERENCES

[1] He Y, Zhang Y, Zhang C, Zhou H. Energy-saving potential of 3D printed concrete building with integrated living wall. Energy and Buildings. 2020 Sep;**222**:110110.
[2] 1.Kareem SA. Additive manufacturing of concrete in construction: potentials and challenges of 3D concrete printing. International Journal of Civil Engineering and Construction. 2022 Jan 1;**1**(1):13–6.
[3] Zhang J, Wang J, Dong S, Yu X, Han B. A review of the current progress and application of 3D printed concrete. Composites Part A: Applied Science and Manufacturing. 2019 Oct;**125**:105533.
[4] Abou Yassin A, Hamzeh F, Al Sakka F. Agent based modeling to optimize workflow of robotic steel and concrete 3D printers. Automation in Construction. 2020 Feb;**110**:103040.
[5] Salet TAM, Ahmed ZY, Bos FP, Laagland HLM. Design of a 3D printed concrete bridge by testing. Virtual and Physical Prototyping. 2018 May 31;**13**(3):222–36.
[6] Kazemian A, Yuan X, Cochran E, Khoshnevis B. Cementitious materials for construction-scale 3D printing: Laboratory testing of fresh printing mixture. Construction and Building Materials. 2017 Aug;**145**:639–47.
[7] Shakor P, Nejadi S, Paul G. A Study into the Effect of Different Nozzles Shapes and Fibre-Reinforcement in 3D Printed Mortar. Materials. 2019 May 26;**12**(10):1708.
[8] Tay YWD, Qian Y, Tan MJ. Printability region for 3D concrete printing using slump and slump flow test. Composites Part B: Engineering. 2019

Oct;**174**:106968.
[9] Zhang Y, Zhang Y, She W, Yang L, Liu G, Yang Y. Rheological and harden properties of the high-thixotropy 3D printing concrete. Construction and Building Materials [Internet]. 2019 Mar 20;**201**:278–85.
[10] Ye J, Cui C, Yu J, Yu K, Dong F. Effect of polyethylene fiber content on workability and mechanical-anisotropic properties of 3D printed ultra-high ductile concrete. Construction and Building Materials. 2021 Apr;**281**:122586.
[11] Zareiyan B, Khoshnevis B. Interlayer adhesion and strength of structures in Contour Crafting - Effects of aggregate size, extrusion rate, and layer thickness. Automation in Construction [Internet]. 2017 Sep [cited 2019 Nov 25];**81**:112–21.
[12] Moelich GM, Kruger J, Combrinck R. Modelling the interlayer bond strength of 3D printed concrete with surface moisture. Cement and Concrete Research. 2021 Dec;**150**:106559.
[13] Kaszyńska M, Skibicki S, Hoffmann M. 3D Concrete Printing for Sustainable Construction. Energies. 2020 Dec 1;**13**(23):6351.
[14] Ding T, Xiao J, Zou S, Wang Y. Hardened properties of layered 3D printed concrete with recycled sand. Cement and Concrete Composites. 2020 Jun;103724.
[15] Hasse JA, Rubin AP, Quintanilha LC, Repette WL. Increasing structuration rate of 3D printable concretes: the effect of viscosity enhancing admixtures. Revista IBRACON de Estruturas e Materiais. 2020;**13**(4).
[16] Xiao J, Zou S, Yu Y, Wang Y, Ding T, Zhu Y, et al. 3D recycled mortar printing: System development, process design, material properties and on-site printing. Journal of Building Engineering. 2020 Nov;**32**:101779.
[17] Ding T, Xiao J, Zou S, Zhou X. Anisotropic behavior in bending of 3D printed concrete reinforced with fibers. Composite Structures. 2020 Dec;**254**:112808.
[18] Ma G, Li Z, Wang L, Wang F, Sanjayan J. Mechanical anisotropy of aligned fiber reinforced composite for extrusion-based 3D printing. Construction and Building Materials. 2019 Mar;**202**:770–83.
[19] Marchment T, Sanjayan J. Bond properties of reinforcing bar penetrations in 3D concrete printing. Automation in Construction. 2020 Dec;**120**:103394.
[20] Pham L, Tran P, Sanjayan J. Steel fibres reinforced 3D printed concrete: Influence of fibre sizes on mechanical performance. Construction and Building Materials. 2020 Jul;**250**:118785.
[21] Rahul AV, Santhanam M. Evaluating the printability of concretes containing lightweight coarse aggregates. Cement and Concrete Composites. 2020 Feb;103570.
[22] Nerella VN, Hempel S, Mechtcherine V. Effects of layer-interface properties on mechanical performance of concrete elements produced by extrusion-based 3D-printing. Construction and Building Materials [Internet]. 2019 Apr;**205**:586–601.
[23] Xiao J, Han N, Zhang L, Zou S. Mechanical and microstructural evolution of 3D printed concrete with polyethylene fiber and recycled sand at elevated temperatures. Construction and Building Materials. 2021 Jul;**293**:123524.
[24] Ye J, Cui C, Yu J, Yu K, Xiao J. Fresh and anisotropic-mechanical properties of 3D printable ultra-high ductile concrete with crumb rubber. Composites Part B: Engineering. 2021 Apr;**211**:108639.
[25] EFNARC. Self Compact. Concrete. 2005;**63**.
[26] Nepomuceno M, Oliveira L, Lopes SMR. Methodology for mix design of the mortar phase of self-compacting concrete using different mineral additions in binary blends of powders. Construction and Building Materials. 2012 Jan;**26**(1):317–26.
[27] Nepomuceno MCS, Pereira-de-Oliveira LA, Lopes SMR. Methodology for the mix design of self-compacting concrete using different mineral additions in binary blends of powders. Construction and Building Materials. 2014 Aug;**64**:82–94.
[28] ABNT NBR NM 248.
[29] ASTM D6913.
[30] ABNT NBR NM 52.
[31] ASTM C128.
[32] ABNT NBR NM 45.
[33] ABNT NBR NM 46.
[34] ABNT NBR NM 23.
[35] ASTM C188.
[36] ABNT NBR 13276 2016.
[37] Le TT, Austin SA, Lim S, Buswell RA, Law R, Gibb AGF, et al. Hardened properties of high-performance printing concrete. Cement and Concrete Research [Internet]. 2012 Mar;**42**(3):558–66.
[38] 1.Soltan DG, Li VC. A self-reinforced cementitious composite for building-scale 3D printing. Cement and Concrete Composites. 2018 Jul;**90**:1–13.
[39] ABNT NBR 15839.
[40] ABNT NBR 7222.
[41] Al Rashid A, Khan SA, G. Al-Ghamdi S, Koç M. Additive manufacturing: Technology, applications, markets, and opportunities for the built environment. Automation in Construction. 2020 Oct;**118**:103268.
[42] Weng Y, Li M, Zhang D, Tan MJ, Qian S. Investigation of interlayer adhesion of 3D printable cementitious material from the aspect of printing process. Cement and Concrete Research. 2021 May;**143**:106386.
[43] Geng Z, Wu P, Pan H, Zheng Q, Zuo W, Zhang W, et al. Robust layer interface in cement additive manufacturing via silicate penetration and precipitation. Materials & design. 2022 Feb 1;**214**:110380–0.
[44] ABNT NBR 13279.
[45] ABNT NBR 9778.
[46] Ma G, Li Z, Wang L. Printable properties of cementitious material containing copper tailings for

extrusion based 3D printing. Construction and Building Materials. 2018 Feb;**162**:613–27.
[47] Shakor P, Nejadi S, Paul G, Malek S. Review of Emerging Additive Manufacturing Technologies in 3D Printing of Cementitious Materials in the Construction Industry. Frontiers in Built Environment. 2019 Jan 23;**4**.
[48] Cardoso FA, John VM, Pileggi RG, Banfill PFG. Characterisation of rendering mortars by squeeze-flow and rotational rheometry. Cement and Concrete Research. 2014 Mar;**57**:79–87.
[49] Nicolini A, Gonçalves Maciel V, da Silva Andrade Neto J, Roca Bragança S, Maldaner Jacobi M. Rheological behavior of fresh latex polymeric mortar by squeeze-flow technique. Construction and Building Materials. 2021 Jan;**267**:121175.
[50] Cardoso FA, John VM, Pileggi RG. Rheological behavior of mortars under different squeezing rates. Cement and Concrete Research. 2009 Sep;**39**(9):748–53.
[51] Panda B, Paul SC, Mohamed NAN, Tay YWD, Tan MJ. Measurement of tensile bond strength of 3D printed geopolymer mortar. Measurement. 2018 Jan;**113**:108–16.
[52] Wolfs RJM, Bos FP, Salet TAM. Hardened properties of 3D printed concrete: The influence of process parameters on interlayer adhesion. Cement and Concrete Research [Internet]. 2019 May;**119**:132–40.
[53] Chen Y, Romero Rodriguez C, Li Z, Chen B, Çopuroğlu O, Schlangen E. Effect of different grade levels of calcined clays on fresh and hardened properties of ternary-blended cementitious materials for 3D printing. Cement and Concrete Composites. 2020 Nov;**114**:103708.
(Rec. 15/12/2022, Rev. 13/09/2023, Ac. 04/11/2023)
(AE: A. E. Martinelli)